Development of a One-Month Long, Westward-Propagating Subtropical Low in Boreal Summer

John Molinari[1] and David Vollaro

Department of Atmospheric and Environmental Sciences

University at Albany, SUNY

Submitted to *Monthly Weather Review*

Submitted May 8, 2017

Revised November 1, 2017

[1]Corresponding author address:

Department of Atmospheric and Environmental Sciences, ES-225

University at Albany/SUNY

1400 Washington Avenue

Albany, NY 12222.

jmolinari@albany.edu

ABSTRACT

A strong MJO event produced an upper tropospheric jet streak in northeast Asia and repeated wavebreaking in the jet exit region along 150°E during July 1988. A midlatitude low moved equatorward and intensified in the presence of bandpass-filtered (15-100 d) Q vector forcing for upward motion associated with the wave breaking. This forced ascent helped to moisten the atmosphere enough to increase the column water vapor to above 55 mm. This value was sufficiently large to support a self-sustaining low even after the upper forcing weakened. The horizontal scale of the Q vector forcing was about 1500 km, consistent with the scale of most favorable convective response to quasi-geostrophic forcing in the subtropics described by Nie and Sobel. The low lasted one month as it moved southwestward, then westward, while remaining north of 20°N. Maximum precipitation along the track of the low exceeded 700 mm, with an anomaly more than 400 mm.

A climatology of long-lasting lows was carried out for the monsoon gyre cases studied previously. During El Niño, long-lasting lows often began near the equator in the central Pacific, and were likely to have a mixed Rossby-gravity wave or equatorial Rossby wave structure. It is speculated that the quasi-biweekly mode, the submonthly oscillation, the 20-25 day mode, and the Pacific-Japan Pattern are each variations on this kind of event. During La Niña, long-lasting lows that originated in middle latitudes were more common. It is argued that these lows from midlatitudes represent a unique disturbance type in boreal summer.

1. Introduction

Yano et al. (2009) noted the dominance of vorticity over divergence in the tropics. Raymond et al. (2015) divided tropical convection into two components: stochastic and predictable, the latter associated with balanced dynamical forcing. The balanced forcing creates a long-lasting cyclonic response, consistent with Yano's findings. Boos et al. (2014) argued that balanced forcing controls the motion of monsoon depressions. These papers suggest that cyclonic disturbances should be common in the tropics and subtropics. The emphasis of this paper is on longer-lasting low pressure areas in boreal summer in the northwest Pacific.

Hartmann et al. (1992) described boreal summer disturbances with 20-25 d periods that first appeared west of the Date Line at the equator, then recurved northward east of the Philippines, and moved poleward beyond 20°N. Molinari et al. (2007) argued that these represented equatorial Rossby (ER) waves turning off the equator as they moved westward. Kikuchi and Wang (2009) described the "quasi-biweekly oscillation" using a bandpass 12-20 d filter, but noted that a 12-30 d filter gave similar results. Like Hartmann et al. (1992), the authors identified disturbances that originated near the equator in the central Pacific in boreal summer (their Fig. 6) that turned poleward and westward with time. Ko et al. (2009; 2012) described a "submonthly oscillation" isolated using a 7-30 d filter. Once again in boreal summer the disturbances initiated at or near the equator, and propagated northwestward east of the Philippines. They were most active during the active (westerly) phase of the MJO in the western Pacific. Finally, the Pacific-Japan Pattern has been isolated using monthly mean fields (Nitta, 1987) and 10-50 d filtered fields (Li et al. 2014). It also exhibits a wave train with northwestward motion east of the Philippines. The characteristics of these disturbances overlap considerably.

Molinari and Vollaro (2012; hereafter MV12) described the structure of a large "monsoon gyre" during summer 1988 that slowly propagated westward north of 20°N. MV12 described the full synoptic variability of the gyre. Its formation represented an extremely complex series of events involving the aggregation of midlatitude cyclonic vorticity maxima and subtropical convectively-generated vorticity. MV12 argued that midlatitude forcing played the most significant role in the disturbance, suggesting such disturbances differ from the near-equatorial origin of those described above.

In the current paper, the previous case study will be re-examined and extended using a bandpass-filtered framework, with considerable simplification and benefit to basic understanding of this event. The large low will be shown to last a month, considerably longer than the 5 days described by MV12. The goals are to understand the mechanisms by which the low formed and maintained itself over such a long period, and where it fits among the hierarchy of disturbances in the northwestern Pacific in boreal summer.

2. Data and methods

Following MV12, operational gridded analyses from the European Center for Medium Range Weather Forecasting (ECMWF) were used to obtain the wind, height, and vorticity fields for the 1988 case study. A climatology of long-lived low pressure areas made use of ERA-Interim analyses (Dee and co-authors 2011). Tropical cyclone positions were obtained from the Joint Typhoon Warning Center and the Japanese Meteorological Agency (JMA). Real-time Multivariate MJO (RMM) values[1] (Wheeler and Hendon 2004) and the OLR-based MJO index

[1] http://www.bom.gov.au/climate/mjo/

(OMI; Kiladis et al. 2014)[2] provided measures of the MJO state. Anomalies from climatology were determined using a 31-year twice daily mean state (1983-2013). Three measures of cloud and precipitation were used:

(i) OLR on a 2.5º grid (Liebman and Smith 1996; and upgraded by George Kiladis, 2003, personal communication). These are used for all 15-100 d filtered fields. Such longer-period oscillations should not be impacted by the six-hour time shifts in the data.

(ii) Daily rainfall data were obtained from the PERSIANN dataset (Ashouri et al. 2015). This is based on hourly data summed over 24-h periods centered at 1200 UTC on a resolution of 0.25°latitude and longitude. PERSIANN allows a better estimate for precipitation than OLR fields.

(iii) Convective activity on individual (unfiltered) daily maps was evaluated using infrared brightness temperature data from the Cloud Archive User Service (CLAUS). Because this is available on a 0.5° latitude-longitude grid eight times daily, it is superior to the other two fields for examining convective distribution evolution in the large low.

The dynamical forcing of vertical motion will be defined using Q vector convergence (Hoskins et al. 1978) following MV12. The formulation uses the quasi-geostrophic formulation for Q vectors, but with geostrophic wind replaced by nondivergent wind (Davies-Jones 1991; Galarneau et al. 2010). This formulation extends the applicability of the results to the subtropics.

Roundy and Frank (2004) used a 15-100 d filter in order to describe westward-propagating intraseasonal oscillations associated with ER waves in boreal winter. The broad filter was required because ER wave speed is comparable to that of the background flow (Kiladis et al.

[2] http://www.esrl.noaa.gov/psd/mjo/mjoindex/

2009). When such a wave encounters strong westerlies, its speed can slow sufficiently to shift it to much longer periods.

Similar issues arose for the large low in this study. Fig. 1 shows weather maps of the cyclone on 28 July at 0000 UTC for two time filter ranges, 15-40 d and 40-100 d. The vorticity maxima for the two filter bands occurred at nearly the same location. Both filter bands revealed large cyclonic disturbances with similar OLR minima equatorward of the center. In addition, the disturbances propagated westward in both filter bands (not shown). Because the two filter bands did not seem separable, all figures shown hereafter represent 15-100 d bandpass-filtered fields. As in previous work (e.g., Molinari et al. 2007), a Lanczos filter has been used for all filter bands.

3. Upstream precursors

The evolution of two MJO indices is displayed in Figure 2 from mid-June to mid-August 1988, prior to and during the life of the cyclone of interest. The RMM and OMI indices present a broadly similar evolution: (i) MJO amplitude above 1 in the second half of June and early July, mostly in phases 8 and/or 1; and (ii) continuous shifts through MJO phases as the cyclone intensified in the northwest Pacific. The major differences in the indices are (i) the large amplitude of OMI during the month of July; and (ii) a more continuous evolution of MJO phase in OMI. Kiladis et al. (2014) argued that OMI was appropriate when examining individual cases in which convective evolution was of interest.

RMM Phase 1 in boreal summer (Wheeler and Hendon 2004; see reproduction in Fig. 10 of Molinari and Vollaro 2017) corresponds to above-average convective heating over the equatorial Bay of Bengal and below-average convection over the maritime continent and the far

western Pacific. Phases 8 and 1 in OMI (available at the web site noted earlier) shows a second maximum in convective forcing near 20°N and 120°E. Bandpass-filtered OLR, velocity potential, and divergent winds at 200 hPa are shown in Fig. 3 for the current case study on 23 June, 1988 at 0000 UTC. The pattern at that time was representative of the entire second half of June. A convective maximum appears at the same longitude and about 5° north of phases 8 and 1 in the OMI composite. Poleward divergent flow north of the convective maximum supported the generation of a westerly jet near 40°N. For this event, the OMI composite provides a superior fit compared to RMM.

Bandpass-filtered (15-100 d) 200 hPa winds (Fig. 4) confirmed a westerly anomaly greater than 25 ms^{-1} over Asia on 7 July in response to the divergent flow. This anomaly pattern, which held throughout the first half of July (not shown), strongly favors wave breaking downwind of such a jet exit region (Takaya and Nakamura 2001). Consistent with this reasoning, MV12 described a series of upper-tropospheric wave breaking events in the northwest Pacific that reached their farthest equatorward penetration on 4, 9, 15, 20, and 27 July 1988, all occurring near 150°E. Due to the lack of a westerly duct (Webster and Holton 1982) at low latitudes, these summer wavebreaking events did not reach within 2000 km of the equator.

The cumulative impact of these events can be seen in the 15-100 d bandpass-filtered Ertel potential vorticity (PV) on the 355K and 340K isentropic surfaces on 14, 20, and 26 July 1988 in Fig. 5. The pressure on the 355K surface above the low was about 170 hPa at 355K, and 340 hPa at 340K. The “L” in these panels represents the center of the low at 850 hPa. On 14 July, the 850 hPa low was found almost directly under the maximum PV at both 355K and 340K. It is notable that the scale of the PV maximum falls in the 1000-2000 km range found by Nie and Sobel (2016) to optimize convective response to quasi-geostrophic forcing in the subtropics.

Six days later, the low still lay under the 355K maximum, but the upper PV anomaly weakened, consistent with destruction of PV aloft by deep convection. By 26 July, only anticyclonic PV existed at 355K. High PV was advected both equatorward and poleward by the strong outflow from above the low. By this last time, the 850 hPa low lay directly under a region of positive PV advection at 340K. The dominant right-hand side term in the quasi-geostrophic omega equation can be written in terms of minus twice the Q vector convergence following Holton's text, but it can also be written in terms of the vertical derivative of potential vorticity advection (i.e., Hoskins et al. 1985, their Eq A7). The two formulations are broadly equivalent, with smaller terms neglected in each case. In essence, upward motion associated with Q vector convergence is driven by upper tropospheric PV advection. It is hypothesized that through such forcing, the upper tropospheric PV supports a strong convective response, and thus the growth and intensification of the low during this period, even though convection appears to destroy the 355K PV maximum over time. This will be addressed further in the following section.

4. Development of a one-month cyclone

Fig. 6 shows the evolution of the disturbance in bandpass-filtered OLR and 850 hPa wind every 4 days from 14 July to 11 August 1988. On 14 July, a midlatitude low existed at 40°N, 151°E. Winds and OLR indicated the presence of an extended confluent region with precipitation east of the low. The northwest Pacific monsoon trough was found near 10°N, its typical location in July (Molinari and Vollaro 2013). Between these regions, a broad anticyclone with little precipitation existed in the subtropics. Four days later (Fig. 6b), the low had shifted about 800 km equatorward and westward. A strong negative OLR anomaly shifted southward with the low, and began to separate from higher latitudes and grow in extent. The equatorward movement of

the low and the separation of the OLR minimum continued on 26-30 July (Fig. 6c,d). The precipitation field of the low began to superpose with that of the background monsoon trough. The low then moved westward and eventually northward by 11 August (Fig. 6e-h).

The large low seen in Fig. 6 existed only in the Northern Hemisphere. No ER-wave type signature was seen in the Southern Hemisphere in either wind or OLR (not shown). Unlike in boreal winter, the midlatitude forcing in this case was not perturbing the equatorial wave guide.

The overall track of the cyclone is given in Fig. 7. This was constructed following Nguyen et al. (2014) by plotting the centroid of the 850 hPa 15-100 d bandpass-filtered height minimum in the vicinity of the low. An apparent jump in the position of the low on 30 July arose because the low became elongated in the east-west direction, with a broader region of minimum height. The low influenced a significant portion of the west Pacific during the four-week period.

Fig. 8 is designed to make connections between upper PV forcing shown earlier in Fig. 5 and the following fields: the Q vector convergence, the ω from ERA-Interim, and the balanced vertical velocity calculated from the Q vector forcing in the quasi-geosptrophic ω equation. This was done by averaging those fields at each level, but only over the region of all grid points connected to the low that experienced an OLR anomaly of less than -20 W m^{-2} (see contiguous orange and warmer shading in Fig. 6). Several striking results are shown in Fig. 8. First, the forcing was by far the largest on 14 July, at the initial time. Second, the forcing was largest in the upper troposphere, consistent with the large 355K PV over the low in Fig. 5. The maximum forcing fell 50% by 20 July, and and an additional 50% by 26 July. The total ω indicated broad ascent through much of the troposphere at the initial time. Thereafter the vertical motion increased at all levels in the convective region even as the forcing decayed. The quasi-geostrophic forcing was much weaker than the total vertical motion, suggesting dominance of

diabatic effects once convection was excited. On 14 July the balanced upward motion was largest in the upper troposphere with a magnitude 30% of the total omega. By 26 July the maximum in balanced vertical motion had descended to the mid troposphere with an intensity just 15% of the total. We hypothesize that convection was excited in response to destabilization of the column by the upward motion.

Fig. 9 displays a Hovmöller diagram of 15-100 d bandpass-filtered 850 hPa meridional wind and OLR. The bold red line represents the track of the low center. Intensification of convection appeared to lead the cyclonic spinup by a few days. The same meridional wind field is overlaid in Fig. 10 with total (i.e., unfiltered) column water vapor (mm; hereafter CWV). Early in the life of the cyclone CWV exceeded 55 mm, and remained high thereafter. Unfiltered values allowed us to evaluate the role of CWV proposed by Peters and Neelin (2006) and Holloway and Neelin (2009), who have noted that above this threshold, moist regions of the tropics tend to be self-sustaining because precipitation rises exponentially with CWV. Hannah et al. (2016) and Allen and Mapes (2017) placed the cutoff at 50-55 mm. These views are supported by the long life of the low as it retained large CWV over several weeks.

5. Broader impacts of the large cyclone

a. Precipitation

The total precipitation from 7/14/88 to 8/12/88 (Fig. 11a) shows a remarkable maximum of over 700 mm that extended zonally south of the track of the low. A separate precipitation maximum associated with the western Pacific monsoon trough near 5°N extended across most of the region. The two precipitation maxima merged somewhat to the west.

The precipitation anomaly from the 31-year climatology (Fig. 11b) reached 517 mm near 20°N, 140°E, indicating that much of the precipitation excess along 20°N arose along and south of the path of the low. The origin of the low as a midlatitude system appeared as an extended southwest-northeast oriented precipitation maximum north of 30°N. During the same period, precipitation was suppressed from its climatological value within the monsoon trough region. The suppression of the monsoon trough is consistent with OMI phases 8-1-2, and might represent the impact of compensating subsidence in the forced upward motion to the north.

b. Tropical cyclone track and definition

Crandall et al. (2014) described the evolution of a complex tropical cyclone that was moving cyclonically around the edges of a large subtropical low in 1989. In real time the warning for TS Ken was ended when the cloud signature seemed to vanish. Six hours later, a new tropical cyclone (TS Lola) was declared at another location. Post processing of the data by JTWC indicated that only one tropical cyclone was present, not two. At one particular time, the center was mislocated by 465 km. Crandall et al. (2014) argued that the interaction of the large low and the tropical cyclone contributed to the mislabeling of the tropical storm.

A similar conundrum arises in the current case. A tropical disturbance was declared by JTWC at 0000 UTC 26 July. The JTWC location of the tropical disturbance at this time ("A" in Fig. 12a) corresponds to the cloudless center of the large low. Maximum convection was found 1000 km from the center of the low, not representative of the structure of a tropical cyclone. By 0600 UTC 27 July (Fig. 12b), the disturbance center was shifted to within 500 km of the maximum convection. By 1800 UTC 29 July (Fig. 12c), a tropical storm had formed east of the large low and began racing northward around the edge of the low. At this time JTWC placed the

center of TS Agnes directly within the convective maximum. The final panel of Fig. 12 indicates that Tropical Storm Agnes was moving away from the large low. Agnes later became an intense subtropical cyclone north of 30°N.

The southeastward JTWC track of the disturbance for three days prior to 29 July was extremely anomalous (Camargo et al. 2007). This track seems misleading, in that the definition of the pre-Agnes disturbance changed with time, from the center of the large low to the local Tropical Storm. Fig. 12 shows almost no change in the position of the strongest convection between 0000 UTC 26 July and 1800 UTC 29 July, even though the tropical disturbance moved nearly 1000 km.

Fig. 12 also shows the existence of multiple convective disturbances rotating around the inner edge of the cloud shield of the large low. These have been described in detail by Lander (1994) and often represent “midget tropical cyclones”. Their formation seems analogous to mesovortices forming on the inner edge of the eye wall in tropical cyclones, but on a larger scale. The existence of a large low with multiple vorticity maxima, some intensifying, some not, on its inner edge continue to provide challenges for operational prediction and tropical cyclone definition in the northwest Pacific. The operational problem of distinguishing large lows from tropical cyclones noted by Lander (1994) still remains.

6. Climatology of large cyclones in the vicinity of monsoon gyres

This study examined the lifetime of a large cyclone that was associated with a monsoon gyre in 1988 by using bandpass filtering. In this section all of the gyres studied by Molinari and Vollaro (2017) will be analyzed in the same manner in order to get a better sense of the typical behavior of these lows. Only JJAS gyres were included to be consistent with the current study.

Only lows lasting at least two weeks were plotted. Fig. 13 shows the tracks of these long-lived lows, divided among La Niña plus ENSO-neutral (top panel) and El Niño (bottom panel). The mean lifetime of these lows was 20.5 days. Many more low-latitude lows were found during El Niño (Fig. 13b). In contrast, 76% of La Niña lows developed poleward of 15°N (Fig. 13a).

7. Discussion

The following sequence of events occurred in the northwest Pacific in June-July 1988:

(i) A strong MJO was active for several weeks over the far western Pacific prior to formation of the large low. Persistent divergent flow from the convection reached 40°N over Asia;

(ii) The Asian upper tropospheric anticyclone intensified, creating an anomalously strong 200 hPa jet near 45°N in northeast Asia;

(iii) Midlatitude wave breaking occurred downwind of the anomalous jet every 5-6 d near 150°E over a 3-week period, repeatedly injecting upper tropospheric PV into the subtropics;

(iv) This sequence of events produced a bandpass-filtered intense PV maximum that moved equatorward in the subtropics. The resulting PV advection created Q-vector convergence forcing for ascent on 14 July;

(v) Bandpass convection and vertical velocity in the subtropics responded quickly to this forcing;

(vi) A large low formed and intensified in the lower troposphere as both the Q-vector convergence and the disturbance shifted equatorward with time;

(vii) The forcing weakened over time (Fig. 8);

(viii) The cyclone maintained its structure for two additional weeks as it moved slowly west-southwestward, then westward. In total it lasted about one month;

(ix) Flow associated with the large cyclone strongly perturbed precipitation and tropical cyclone tracks.

a. What is the nature of these disturbances?

In the Introduction we described the many labels given to large northwestward-moving lows east of the Philippines. Hartmann et al.'s (1992) 20-25 day mode, the Kikuchi and Wang (2009) description of the quasi-biweekly mode, and the Ko et al. (2009) submonthly oscillation all display large lows originating near the equator in the central west Pacific and moving poleward in the far western Pacific. In addition, the structure of these low-latitude lows usually resembled either ER waves (Molinari et al. 2007) or MRG waves (Dickinson and Molinari 2002). During El Niño (Fig. 13b), it is conceivable that all of these disturbances overlap, and there might be redundancy in the naming conventions. In contrast, during La Niña (Fig. 13a), 76% of these large lows formed poleward of 15°N. We argue that this represents a unique form of subtropical low that is forced from middle latitudes.

Moist subtropical lows have been described with a variety of labels: equatorial wave modes, tropical depressions and cyclones, monsoon lows (see Hurley and Boos 2015; Ditchek et al. 2016), monsoon depressions (Boos et al. 2014 and references within), and monsoon gyres (Lander 1994; Molinari and Vollaro 2017; Papin et al. 2017). All of these disturbances are coupled to convection. Lifetimes of these disturbances range from just a couple of days for

monsoon lows, to multiple days for tropical cyclones and monsoon depressions and gyres. They contribute a significant fraction of precipitation, especially over land areas, and can be responsible for substantial flooding over land (Papin et al. 2017). What makes the disturbance in this study unusual is its large horizontal scale and long duration versus most of the monsoonal lows described above, which created significant precipitation and tropical cyclone track anomalies.

b. Why does the low last for several weeks?

We next provide three hypotheses for the long lifetime of this low. First, repeated wave breaking over several weeks supplied the 15-100 d forcing for the disturbance. If only a single wave-breaking event reached the subtropics, the forcing would likely not have been sufficiently persistent, and no long-lasting low might have formed. Strong evidence supports the role of the MJO in creating this favorable background state. Because breaking midlatitude waves in the northwest Pacific peak in boreal summer (Postel and Hitchman 1999), this type of disturbance might be most common during that season.

Second, the midlatitude forcing as measured by upper tropospheric PV (Fig. 5) existed on a scale of about 1000-1500 km. Nie and Sobel (2016) argued that the strength of the coupling between convection and vertical motion is set by the characteristic scale of the quasi-geostrophic forcing. It is notable that the scale of the forcing in Fig. 5 falls within the optimum 1000-2000 km optimum scale of Nie and Sobel (2016). In support of this, Figs. 6 and 8 showed an extremely rapid convective and vertical motion response even to the weak forcing from the Q vector convergence.

The final aspect of the long-lived low was the rapid increase of CWV to above 50-55 mm as a result of the optimum response to forcing. The resulting high-CWV low lasted for several weeks, consistent with the observed persistence of moist precipitating regions in the tropics (Hannah et al. 2016; Allen and Mapes 2017). In sum, the strong upstream MJO, the favorable scale of wave breaking, and the buildup in CWV all played critical roles in the long life of the low.

Acknowledgments. We greatly appreciate thorough and constructive comments by Dr. George Kiladis, Dr. Jie Nie, and an anonymous reviewer. This work was supported by NSF Grant AGS1249732. ECMWF gridded analyses were obtained from the National Center for Atmospheric Research.

References

Allen, T. L., and B.E. Mapes 2017: The late-spring Caribbean rain-belt: climatology and dynamics. *Inter. J. Climatology*, DOI:10.1002/joc.5136.

Ashouri, H., K.-L. Hsu, S. Sorooshian, D.K. Braithwaite, K.R. Knapp, L.D. Cecil, B.R. Nelson, and O.P. Prat, 2015: PERSIANN-CDR: Daily precipitation climate data record from multisatellite observations for hydrological and climate studies. *Bull. Amer. Meteor. Soc.*, **96**, 69–83.

Boos, W.R., J.V. Hurley, and V.S. Murthy, 2014: Adiabatric westward drift of Indian monsoon depressions. *Quart. J. Roy. Meteor. Soc.*, **140**, DOI:10.1002/qj.2454.

Camargo, S.J., A.W. Robertson, S.J. Gaffney, P. Smyth, and M. Ghil, 2007: Cluster analysis of typhoon tracks. Part I: General properties. *J. Clim.*, **20**, 3635-3653.

Crandall, B., J. Molinari, and D. Vollaro, 2014: Forecasting challenges associated with tropical cyclones within subtropical gyres. *Wea. Forecasting*, **29**, 99-114.

Davies-Jones, R., 1991: The frontogenetical forcing of secondary circulations. Part I: The duality and generalization of the Q vector. *J. Atmos. Sci.*, **48**, 497-509.

Dee, D.P., and Coauthors, 2011: The ERA-Interim reanalysis: Configuration and performance of the data assimilation system. *Quart. J. Roy. Meteor. Soc.*, **137**, 553-597.

Dickinson, M.J., and J. Molinari, 2002: Mixed Rossby-gravity waves and western Pacific tropical cyclogenesis. Part I: Synoptic evolution. *J. Atmos. Sci.*, **59**, 2183-2196.

Ditchek, S.D., W.R. Boos, S.J. Camargo, and M.K. Tippett 2016: A genesis index for monsoon disturbances. *J. Clim.*, **29**, 5189-5203.

Galarneau, T.J., Jr., L.F. Bosart, and R.S. Schumacher, 2010: Predecessor rain events ahead of tropical cyclones. *Mon. Wea. Rev.*, **138**, 3272-3297.

Hannah, W.M., B.E. Mapes, and J.S. Elsaesser, 2016: A Lagrangian view of moisture dynamics during DYNAMO. *J. Atmos. Sci.,* **73**, 1967-1985.

Hartmann, D.L., M.L. Michelsen, and S.A. Klein, 1992: Seasonal variations of tropical intraseasonal oscillations: a 20-25 day oscillation in the western Pacific. *J. Atmos. Sci.*, **49**, 1277-1289.

Holloway, C. E. and J. D. Neelin, 2009: Moisture vertical structure, column water vapor, and tropical deep convection. *J. Atmos. Sci.*, **66**, 1665-1683. doi: 10.1175/2008JAS2806.

Hoskins, B.J., I. Draghici, and H.C. Davies, 1978: A new look at the ω-equation. *Quart. J. Roy. Meteor. Soc.*, **104**, 31-38.

Hoskins, B.J., M.E. McIntyre, and A.W. Robertson, 1985: On the use and significance of isentropic potential vorticity maps. *Quart. J. Roy. Meteor. Soc.*, **111**, 877-946.

Hurley, J.V., and W.R. Boos, 2015: A global climatology of monsoon low-pressure systems. *Quart. J. Roy. Meteor. Soc.*, **141**, 1049-1064.

Kikuchi, K., and B. Wang, 2009: Global perspective of the quasi-biweekly oscillation. *J. Clim.*, **22**, 1340-1359.

Kiladis, G.N., M.C. Wheeler, P.T. Haertel, K.H. Straub, and P.E. Roundy, 2009: Convectively-coupled equatorial waves. *Rev. Geophys.*, **47**, 1-42.

Kiladis, G.N., J. Dias, K.H. Straub, M.C. Wheeler, S.N. Tulich, K. Kikuchi, K.M. Weickmann, and M.J Ventrice, 2014: A comparison of OLR and circulation-based indices for tracking the MJO. *Mon. Wea. Rev.*, **142**, 1697-1715.

Ko, K.-C., and H.-H. Hsu, 2009: ISO modulation on the submonthly wave pattern and recurving tropical cyclones in the tropical western north Pacific. *J. Clim.*, **25**, 8591-8610.

Ko, K.-C., H.-H. Hsu, and C. Chou, 2012: Propagation and maintenance mechanism of the TC/submonthl wave pattern and TC feedback in the western north Pacific. *J. Clim.*, **25**, 8591-8610.

Lander, M. A., 1994: Description of a monsoon gyre and its effects on the tropical cyclones in the western north Pacific during August 1991. *Wea. Forecasting*, **9**, 640–654.

Li, R.C.Y., W. Zhou, and T. Li, 2014: Influences of the Pacific-Japan teleconnection pattern on synoptic-scale variability in the western North Pacific. *J. Clim.*, **27**, 140-154.

Liebmann, B., and C. Smith, 1996: Description of a complete (interpolated) outgoing longwave radiation dataset. *Bull. Amer. Meteor. Soc*., **77**, 1275-1276.

Molinari, J., K. Lombardo, and D. Vollaro, 2007: Tropical cyclogenesis within an equatorial Rossby wave packet. *J. Atmos. Sci.*, **64**, 1301-1317.

Molinari, J., and D. Vollaro, 2012: A subtropical cyclonic gyre associated with interactions of the MJO and the midlatitude jet. *Mon. Wea. Rev.*, **140**, 343-357.

Molinari, J., and D. Vollaro, 2013: What percentage of western north Pacific tropical cyclones form within the monsoon trough? *Mon. Wea. Rev.*, **141**, 499-505.

Molinari, J., and D. Vollaro, 2017: Monsoon gyres of the northwest Pacific: Influences of ENSO, the MJO, and the Pacific-Japan pattern. *J. Clim.*, **30**, 1765-1777.

Nguyen, L., J. Molinari, and D. Thomas, 2014: Evaluation of tropical cyclone center identification methods in numerical models. *Mon. Wea. Rev.*, **142**, 4326-4339.

Nie, J., and A.H. Sobel, 2016: Modeling the interaction between quasigeostrophic vertical motion and convection in a single column. *J. Atmos. Sci.*, **73**, 1101-1117.

Nitta, T., 1987: Convective activities in the tropical western Pacific and their impact on the Northern Hemisphere summer circulation. *J. Meteor. Soc. Japan*, **65**, 373-390.

Papin, P.P., L.F. Bosart, and R.D. Torn, 2017: A climatology of central American gyres. *Mon. Wea. Rev.*, **141**, 1983-2000.

Peters, O., and J.D. Neelin, 2006: Critical phenomena in atmospheric precipitation. *Nature Physics*, **2**, 393-396, doi:10.1038/nphys314.

Postel, G.A., and M.H. Hitchman, 1999: A climatology of Rossby wave breaking along the subtropical tropopause. *J. Atmos. Sci.*, **56**, 359-373.

Raymond, D. J., Z. Fuchs, S. Gjorgjievska, S. L. Sessions, 2015: Balanced dynmaics and convection in the tropical atmosphere. *Model. Earth Syst.*, **7**, doi:10.1002/2015MS000467.

Roundy, P.E., and W.M. Frank, 2004: Effects of low-freequency wave interactions on intraseasonal oscillations. *J. Atmos. Sci.*, **61**, 3025-3040.

Takaya, K., and H. Nakamura, 2001: A formulation of a phase-independent wave-activity flux for stationary and migratory quasigeostrophic eddies on a zonally varying basic flow. *J. Atmos. Sci*., **58**, 608-627.

Webster, P. J. and J. R. Holton, 1982: Wave propagation through a zonally varying basic flow: The influences of mid-latitude forcing in the equatorial regions. *J. Atmos. Sci.*, **39**, 722-733.

Wheeler, M.C., and H.H. Hendon, 2004: An all-season real-time multivariate MJO index: Development of an index for monitoring and prediction. *Mon. Wea. Rev.*, **132**, 1917-1932.

Yano, J.-I., S. Mulet, and M. Bonazzola, 2009: Tropical large-scale circulations: asymptotically non-divergent? *Tellus*, **61A**, 417-427.

Figure Legends

Figure 1. OLR (W m^{-2}), 850 hPa vorticity (only positive contours shown, starting at 5 X 10^{-6} s^{-1}, in increments of 10 X 10^{-6} s^{-1}) and wind (vectors) on 28 July 1988 at 0000 UTC. (a) 15-40 d filter; (b) 40-100 d filter. Vectors less than 1 m s^{-1} are not plotted. The "C" symbols represent the locations of vorticity maxima.

Figure 2. Phase and amplitude of the MJO as determined by (a) the RMM index; and (b) the OMI index. The values extend over the life of the large low, from 12 June to 13 August.

Figure 3. 15-100 d bandpass-filtered OLR (shaded for negative anomalies only), velocity potential (units 10^6 m^2 s^{-1}), and divergent wind vectors (under 1 m s^{-1} not plotted) on 0000 UTC 23 June. This pattern is relevant throughout the second half of June, and resembles the OMI composites of Kiladis et al. (2014).

Figure 4. Bandpass-filtered 200 hPa wind vectors and wind speed (shaded; increment 5 m s^{-1}) at 1200 UTC 7 July 1988, the time of the largest zonal wind anomaly over northeast Asia.

Figure 5. Bandpass-filtered Ertel potential vorticity (shaded for values > 1 X 10^{-7} m^2 K s^{-1} kg^{-1} only) and wind on the 355K (left panels) and 340K (right panels) isentropic surfaces at 0000 UTC on 14, 20, and 26 July 1988. The "L" refers to the center of the large low at 850 hPa.

Figure 6. 15-100 day bandpass-filtered OLR (W m^{-2}; shading for negative anomalies only) and 850 hPa wind vectors (not plotted for less than 1 m s^{-1}) at 0000 UTC. (a) 14 July; (b) 18 July; (c) 22 July (d) 26 July; (e) 30 July; (f) 3 August; and (g) 7 August; and (h) 11 August 1988. The "L" refers to the location of the center of the large low at 850 hPa.

Figure 7. Once daily (0000 UTC) locations of the centroid of the bandpass-filtered 850 hPa height minima in the cyclone.

Figure 8. Top panel: 15-100 d bandpass-filtered Q-vector convergence (black line; 10^{-19} m s^{-1} kg^{-1}) as a function of height for 14 July 1988. The values shown represent the mean Q vector convergence over the region where bandpass-filtered OLR fell below -20 W m^{-2}, i.e., within the contiguous active convective regions of the low seen in Fig. 6. Also shown are the vertical variation of vertical velocity from the ECMWF gridded analyses, and the balanced vertical velocity from the quasi-geostrophic ω over the same region, calculated in response to the Q vector convergence (both in μbar s^{-1}). Middle and lower panels: same, but for 20 and 26 July 1988, respectively.

Figure 9. Hovmöller diagram of 15-100 d bandpass filtered OLR (shading; only negative anomalies shown) and meridional wind (contours; dashed are negative; increment 1 m s^{-1}). The bold red line indicates the zero meridional wind contour in the disturbance. Each field is averaged from 19° to 29°N.

Figure 10. As in Fig. 8, but with *unfiltered* column water vapor (shading; mm) overlaid on the bandpass-filtered meridional wind.

Figure 11. a. Total precipitation (mm) from the PERSIANN data, summed from 7/14 to 8/12/88; (b) precipitation anomaly from the 1983 – 2013 climatology during the same period.

Figure 12. Unfiltered CLAUS infrared brightness temperature fields, shaded only for values below zero, and 850 hPa unfiltered wind field. (a) 0000 UTC 26 August; (b) 0600 UTC 27 August; (c) 1800 UTC 29 August; and (d) 0600 UTC 30 August. The symbol "A" indicates the center position of TS Agnes as determined by JTWC post-season processing.

Figure 13. Tracks of large cyclones lasting more than two weeks using the same methods as in Fig. 7. All JJAS long-lasting lows associated with the monsoon gyres studied by Molinari and Vollaro (2017) were examined. (a) La Niña plus ENSO neutral tracks, using the ENSO

definition of Molinari and Vollaro (2017). (b) El Niño tracks. An **X** indicates the initial location for each low.

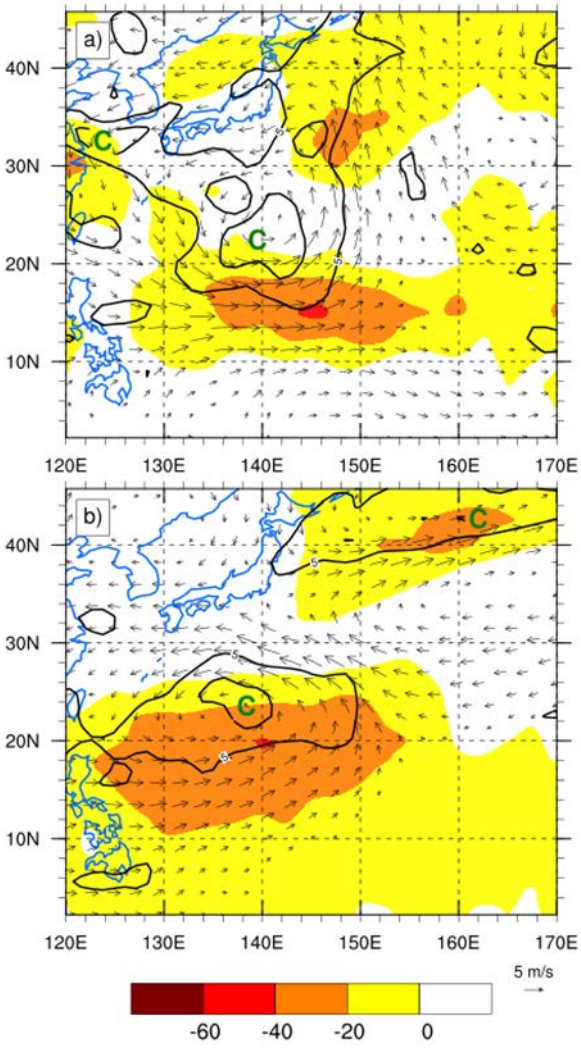

Figure 1. OLR (W m^{-2}), 850 hPa vorticity (only positive contours shown, starting at 5 X 10^{-6} s^{-1}, in increments of 10 X 10^{-6} s^{-1}) and wind (vectors) on 28 July 1988 at 0000 UTC. (a) 15-40 d filter; (b) 40-100 d filter. Vectors less than 1 m s^{-1} are not plotted. The "C" symbols represent the locations of vorticity maxima.

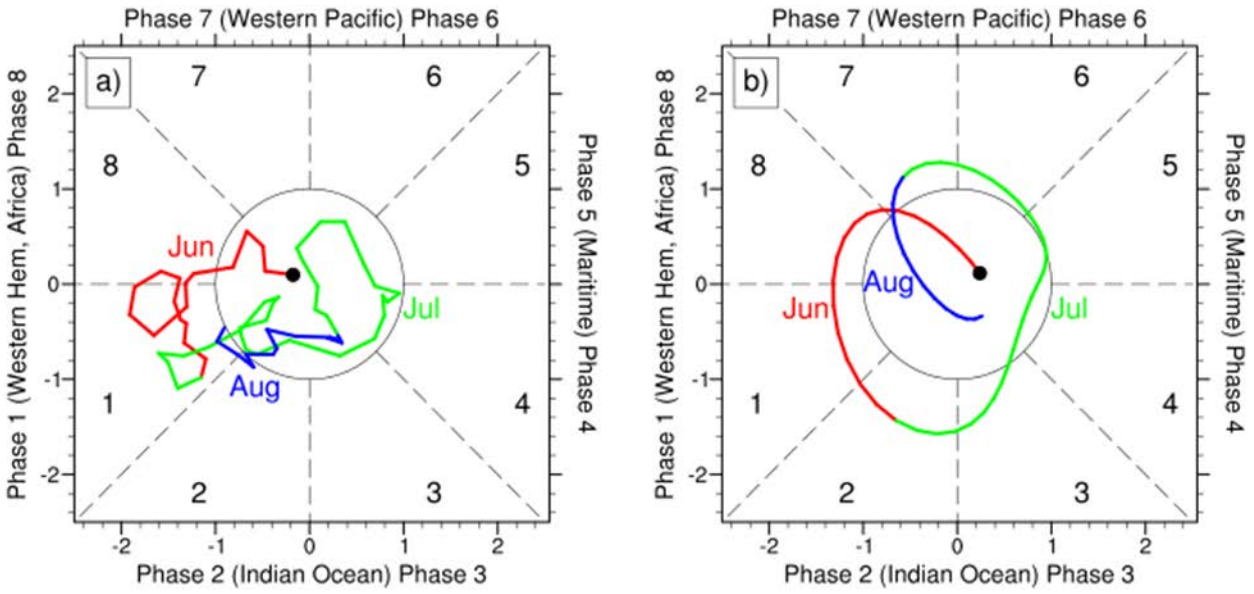

Figure 2. Phase and amplitude of the MJO as determined by (a) the RMM index; and (b) the OMI index. The values extend over the life of the large low, from 12 June to 13 August.

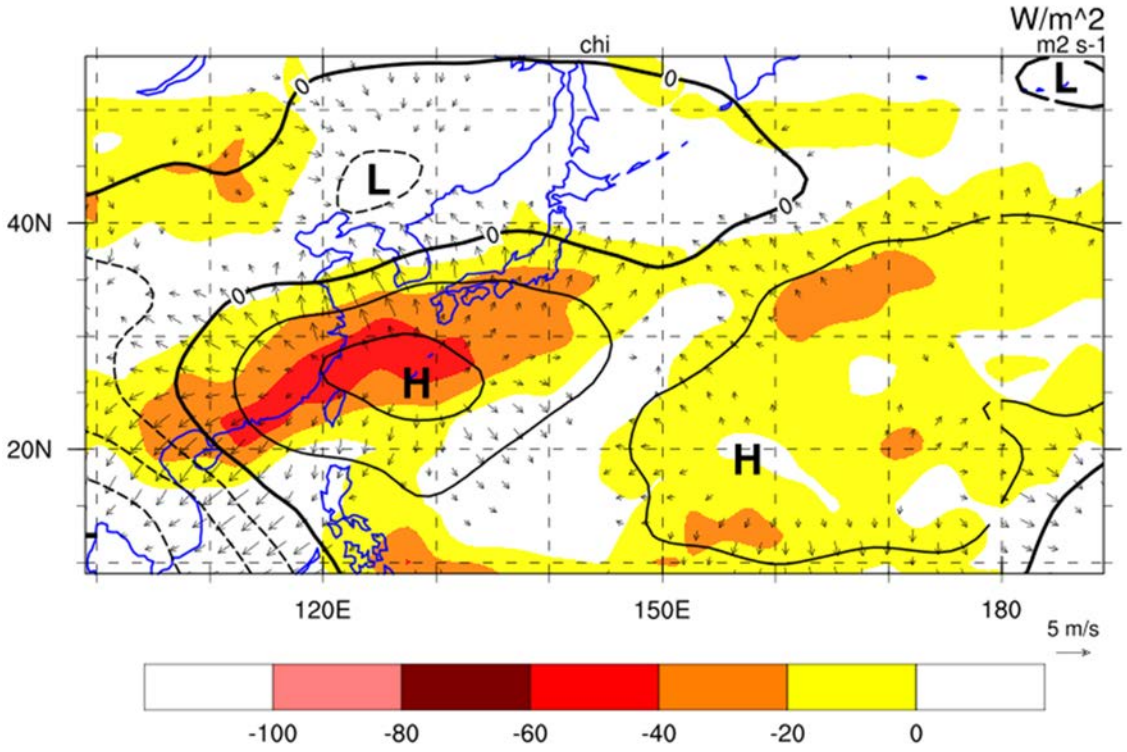

Figure 3. 15-100 d bandpass-filtered OLR (shaded for negative anomalies only), velocity potential (units 10^6 m^2 s^{-1}), and divergent wind vectors (under 1 m s^{-1} not plotted) on 0000 UTC 23 June. This pattern is relevant throughout the second half of June, and resembles the OMI composites of Kiladis et al. (2014).

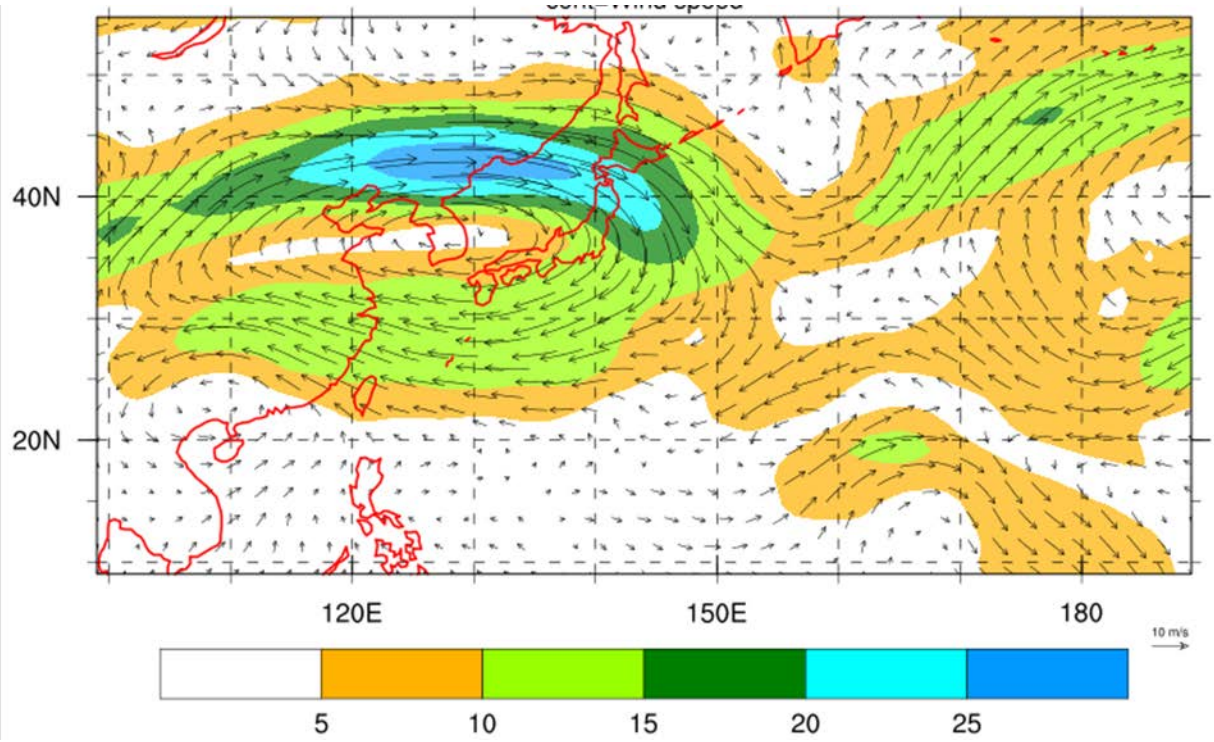

Figure 4. Bandpass-filtered 200 hPa wind vectors and wind speed (shaded; increment 5 m s^{-1}) at 1200 UTC 7 July 1988, the time of the largest zonal wind anomaly over northeast Asia.

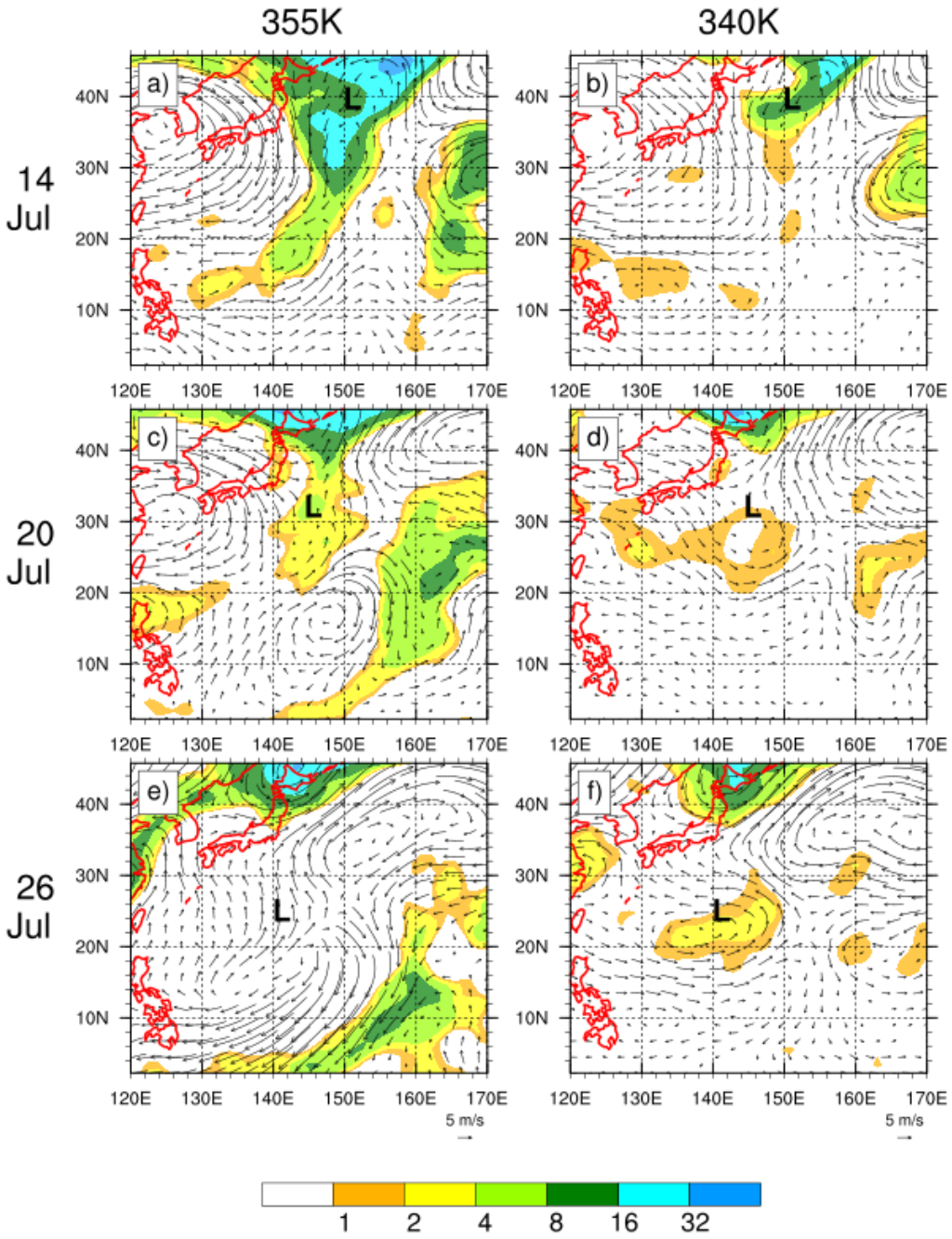

Figure 5. Bandpass-filtered Ertel potential vorticity (shaded for values > 1 X 10^{-7} m^2 K s^{-1} kg^{-1} only) and wind on the 355K (left panels) and 340K (right panels) isentropic surfaces at 0000 UTC on 14, 20, and 26 July 1988. The "L" refers to the center of the large low at 850 hPa.

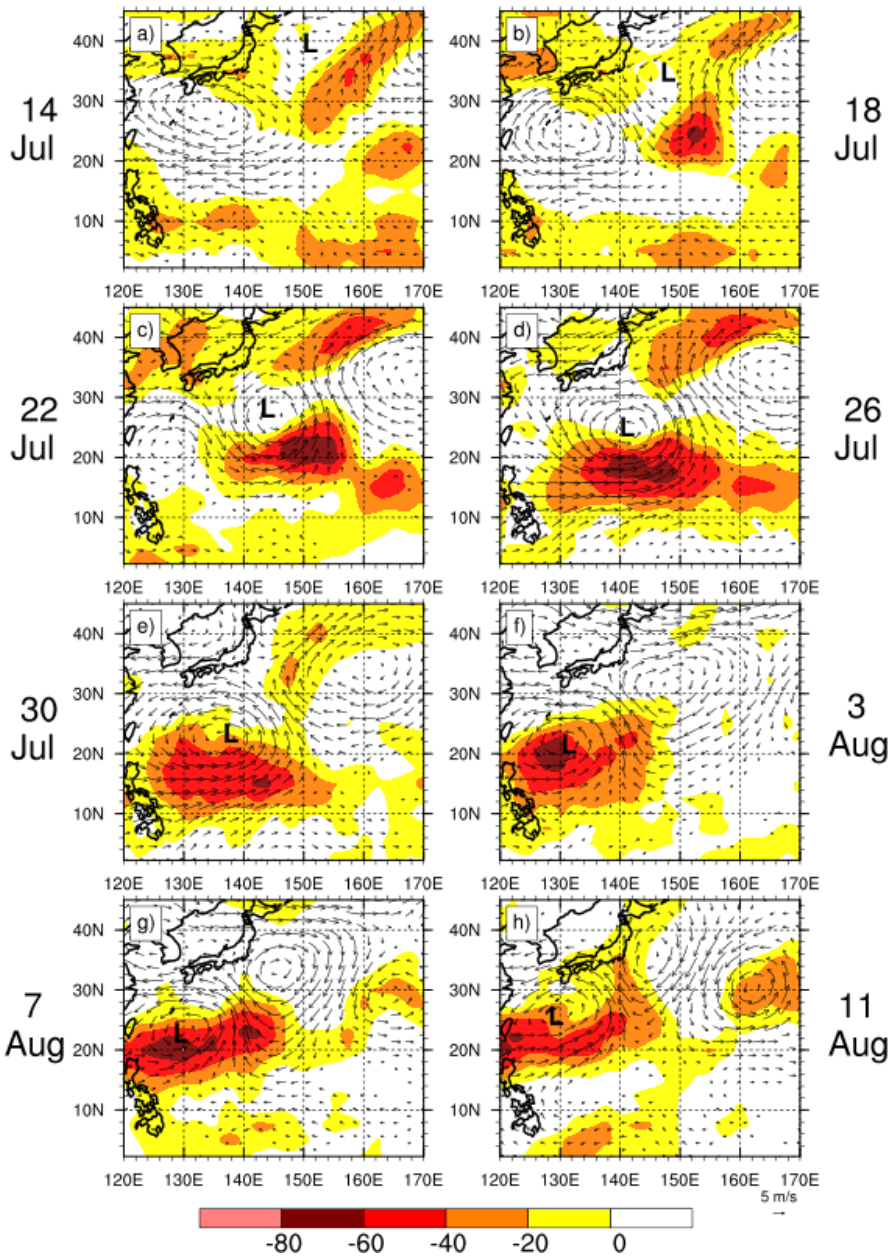

Figure 6. 15-100 day bandpass-filtered OLR (W m^{-2}; shading for negative anomalies only) and 850 hPa wind vectors (not plotted for less than 1 m s^{-1}) at 0000 UTC. (a) 14 July; (b) 18 July; (c) 22 July (d) 26 July; (e) 30 July; (f) 3 August; and (g) 7 August; and (h) 11 August 1988. The "L" refers to the location of the center of the large low at 850 hPa.

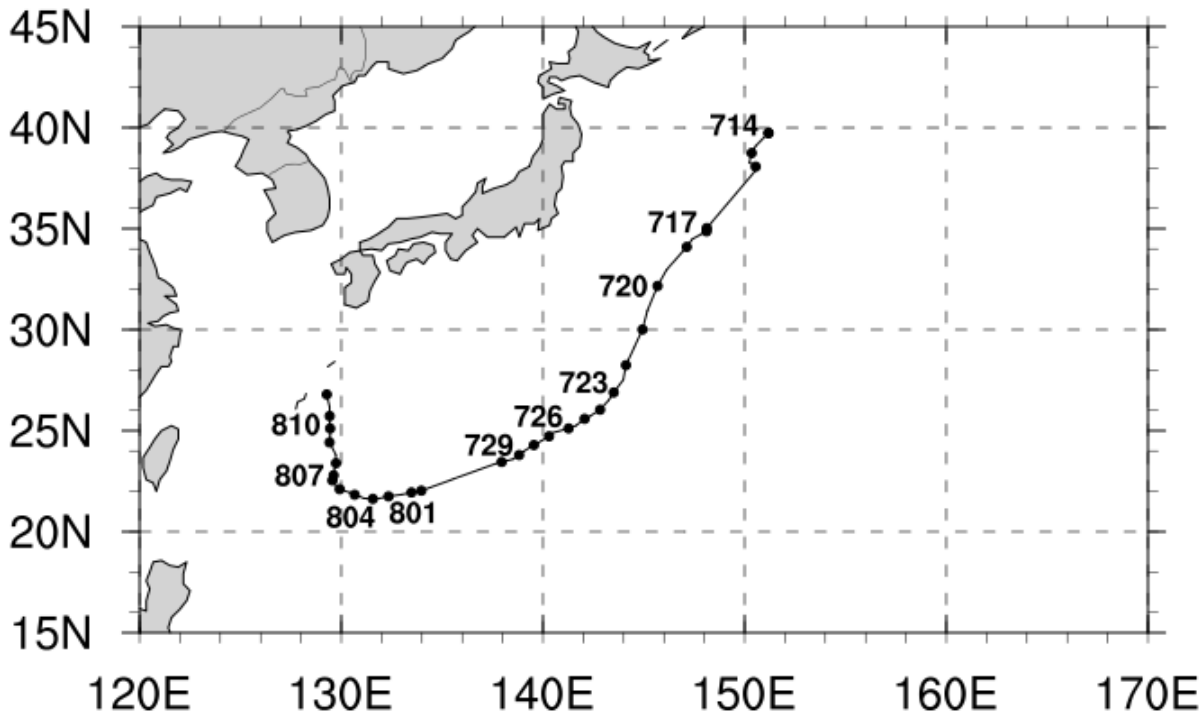

Figure 7. Once daily (0000 UTC) locations of the centroid of the bandpass-filtered 850 hPa height minima in the cyclone.

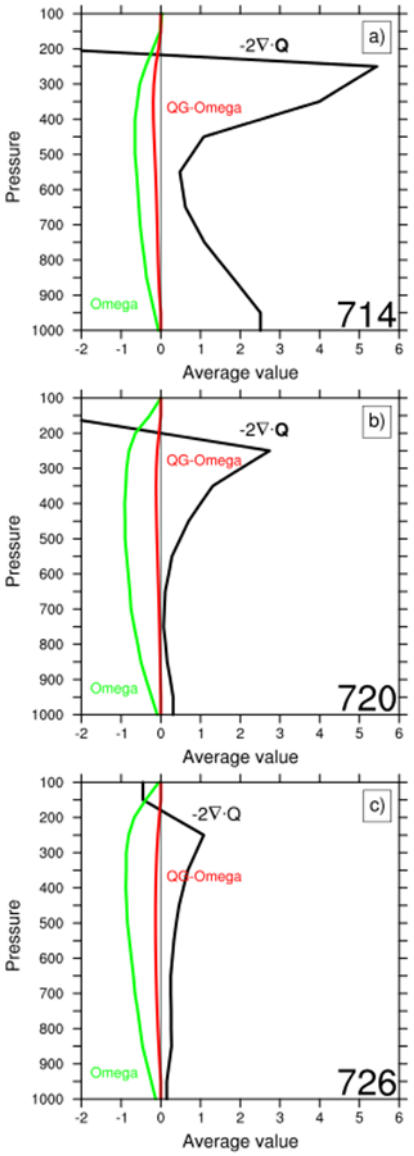

Figure 8. Top panel: 15-100 d bandpass-filtered Q-vector convergence (black line; 10^{-19} m s^{-1} kg^{-1}) as a function of height for 14 July 1988. The values shown represent the mean Q vector convergence over the region where bandpass-filtered OLR fell below -20 W m^{-2}, i.e., within the contiguous active convective regions of the low seen in Fig. 6. Also shown are the vertical variation of vertical velocity from the ECMWF gridded analyses, and the balanced vertical velocity from the quasi-geostrophic ω over the same region, calculated in response to the Q vector convergence (both vertical velocity fields in μbar s^{-1}). Middle and lower panels: same, but for 20 and 26 July 1988, respectively.

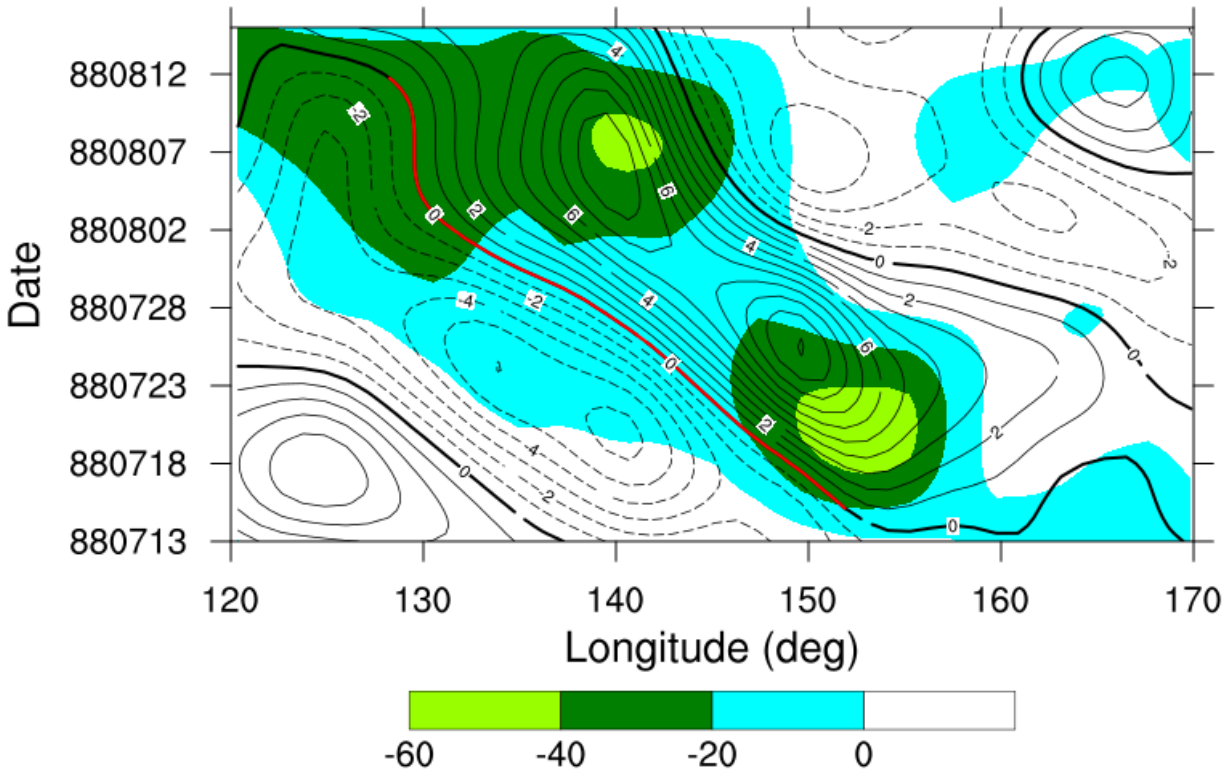

Figure 9. Hovmöller diagram of 15-100 d bandpass filtered OLR (shading; only negative anomalies shown) and meridional wind (contours; dashed are negative; increment 1 m s^{-1}). The bold red line indicates the zero meridional wind contour in the disturbance. Each field is averaged from 19° to 29°N.

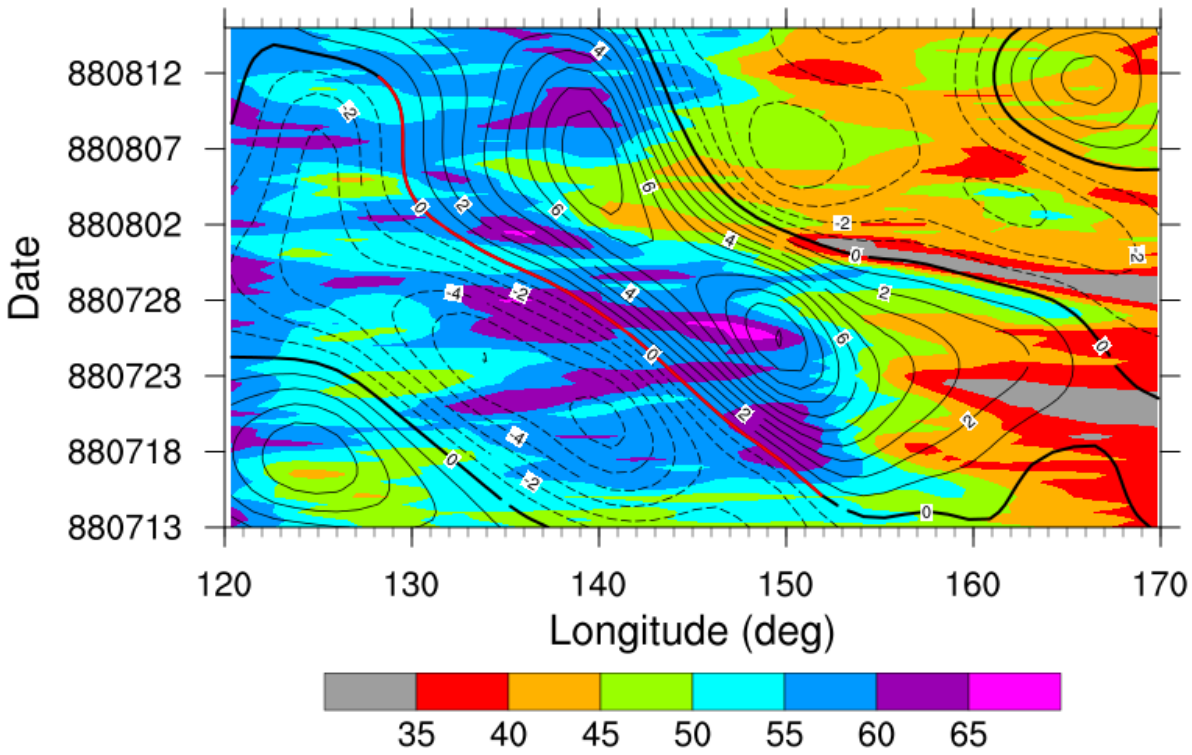

Figure 10. As in Fig. 8, but with *unfiltered* column water vapor (shading; mm) overlaid on bandpass-filtered meridional wind.

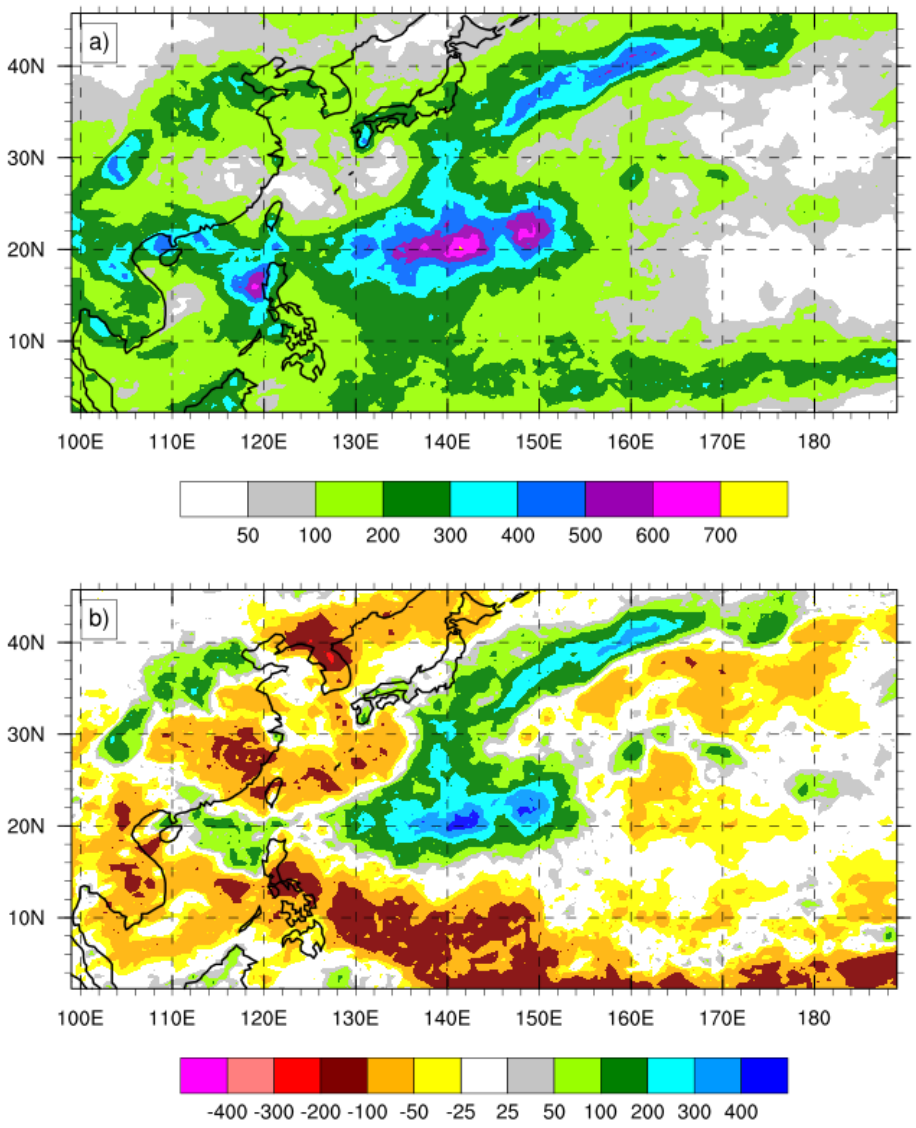

Figure 11. a. Total precipitation (mm) from the PERSIANN data, summed from 7/14 to 8/12/88; (b) precipitation anomaly from the 1983 – 2013 climatology during the same period.

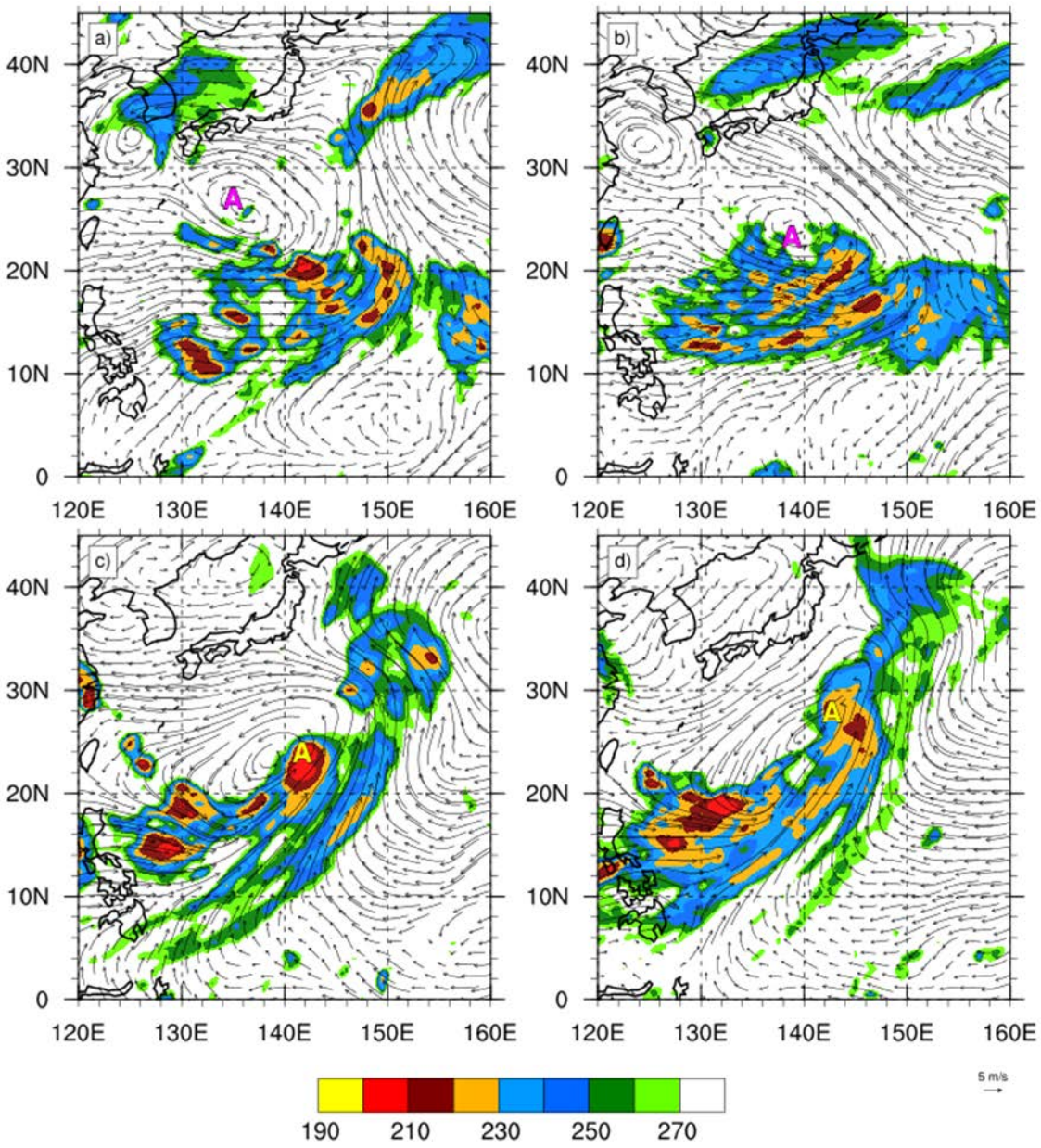

Figure 12. Unfiltered CLAUS infrared brightness temperature fields, shaded only for values below zero, and 850 hPa unfiltered wind field. (a) 0000 UTC 26 August; (b) 0600 UTC 27 August; (c) 1800 UTC 29 August; and (d) 0600 UTC 30 August. The symbol "A" indicates the center position of TS Agnes as determined by JTWC post-season processing.

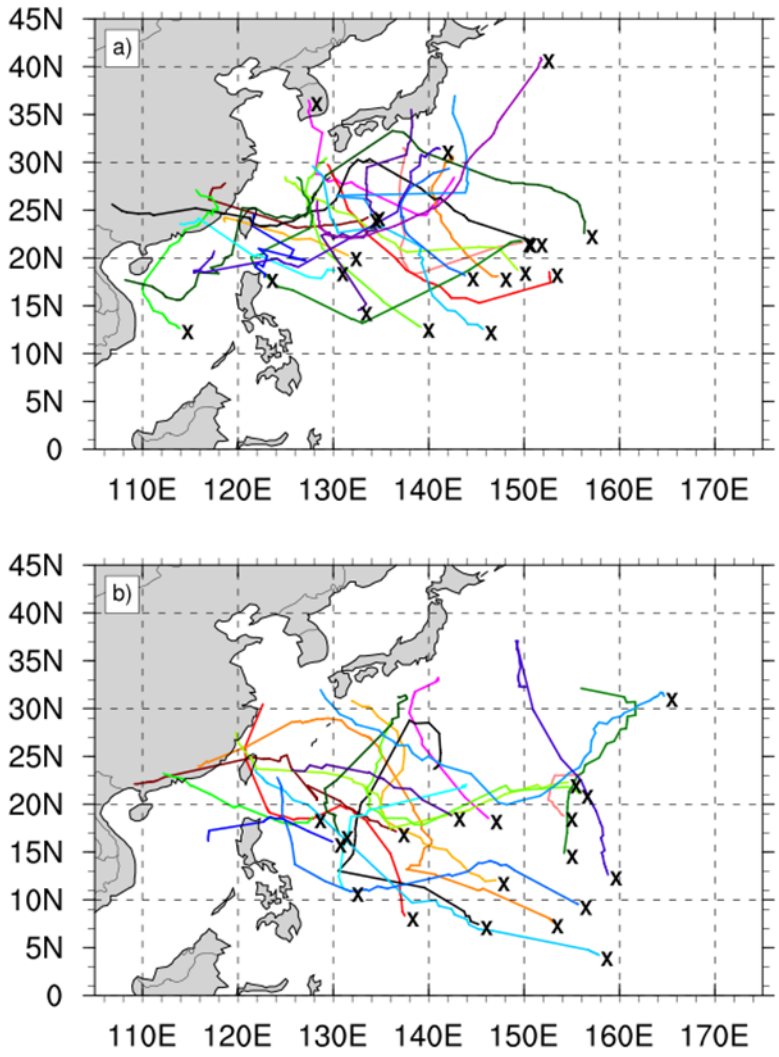

Figure 13. Tracks of large cyclones lasting more than two weeks using the same methods as in Fig. 7. All JJAS long-lasting lows associated with the monsoon gyres studied by Molinari and Vollaro (2017) were examined. (a) La Niña plus ENSO neutral tracks, using the ENSO definition of Molinari and Vollaro (2017). (b) El Niño tracks. An **X** indicates the initial location for each low.